Combined Monte Carlo and molecular dynamics simulation of hydrated 18:0 sphingomyelin–cholesterol lipid bilayers

ARTICLE *in* THE JOURNAL OF CHEMICAL PHYSICS · JUNE 2004

Impact Factor: 2.95 · DOI: 10.1063/1.1724814 · Source: PubMed

2 AUTHORS:

George Khelashvili
Cornell University
59 PUBLICATIONS **709** CITATIONS
SEE PROFILE

Hugh L Scott
Illinois Institute of Technology
84 PUBLICATIONS **2,687** CITATIONS
SEE PROFILE

Combined Monte Carlo and molecular dynamics simulation of hydrated 18:0 sphingomyelin–cholesterol lipid bilayers

George A. Khelashvili and H. L. Scott[a)]
Department of Biological, Chemical and Physical Sciences, Illinois Institute of Technology, Chicago, Illinois 60616

(Received 23 January 2004; accepted 4 March 2004)

We have carried out atomic level molecular dynamics and Monte Carlo simulations of hydrated 18:0 sphingomyelin (SM)–cholesterol (CHOL) bilayers at temperatures of 20 and 50 °C. The simulated systems each contained 266 SM, 122 CHOL, and 11861 water molecules. Each simulation was run for 10 ns under semi-isotropic pressure boundary conditions. The particle-mesh Ewald method was used for long-range electrostatic interactions. Properties of the systems were calculated over the final 3 ns. We compare the properties of 20 and 50 °C bilayer systems with each other, with experimental data, and with experimental and simulated properties of pure SM bilayers and dipalmitoyl phospatidyl choline (DPPC)–CHOL bilayers. The simulations reveal an overall similarity of both systems, despite the 30 °C temperature difference which brackets the pure SM main phase transition. The area per molecule, lipid chain order parameter profiles, atom distributions, and electron density profiles are all very similar for the two simulated systems. Consistent with simulations from our lab and others, we find strong intramolecular hydrogen bonding in SM molecules between the phosphate ester oxygen and the hydroxyl hydrogen atoms. We also find that cholesterol hydroxyl groups tend to form hydrogen bonds primarily with SM carbonyl, methyl, and amide moieties and to a lesser extent methyl and hydroxyl oxygens. [DOI: 10.1063/1.1724814]

INTRODUCTION

Because cholesterol is a major constituent of eukaryotic cell membranes, the manner by which cholesterol affects the structure of lipid bilayers has been studied extensively.[1–8] These studies have established that one of the major effects of cholesterol incorporation in phospholipid monolayer and bilayer model membranes is a broadening and eventual elimination of the cooperative gel-to-liquid-crystalline phase transition. Instead, cholesterol gives rise to a new state with an intermediate degree of organization, which has come to be known as the ''liquid ordered'' phase. The liquid ordered phase has many properties in common with the usual fluid phase: lipid molecules undergo rapid axially symmetric reorientation about their long axis (however the reorientational rates are lower at high cholesterol concentrations than they are for the pure lipid), and the rate of lateral diffusion is comparable to that observed in the fluid phase. The major difference seems to be that the phospholipid chains are more ordered in the liquid ordered phase compared to the normal fluid lipid bilayer phase.

The effect of cholesterol on the lateral organization of multicomponent membranes is a topic of high interest in membrane biophysics. An increasing number of experiments have demonstrated the existence of sphingolipid- and cholesterol-enriched nano-domains known as ''functional rafts'' in the plasma and possibly other membranes of animal cells.[9–11] Rafts have subsequently been identified as important membrane structural components in signal transduction,[12–15] protein transport,[16–18] and sorting of membrane components.[19–21] Due to the importance of the problem, sphingomyelin (SM)–cholesterol (CHOL) complexes have been comprehensively studied using differential scanning calorimetry,[6,7,22,23] x-ray diffraction,[6,7] solid-state NMR,[24,25] and fluorescence-quenching methods.[26–28] Using scanning calorimetry experiments Nyholm *et al.*[23] established that at 25 mol % CHOL the main phase transition in 16:0 SM–CHOL bilayers disappeared and only the sterol-induced transition (phase separation into cholesterol-rich membrane domains) remained. They also report that for CHOL concentration as low as 10%, the pretransition in the system was no longer observable. Using differential scanning calorimetry McMullen *et al.*[29] found that in phosphatidylcholine membranes the total enthalpy of the transition decreased with increasing CHOL concentration. Using x-ray diffraction, Maulik *et al.* found that at 50% mol CHOL concentration the peak-to-peak distance in electron density profiles of hydrated 16:0 palmitoylsphingomyelin (PSM)–CHOL bilayers at 29 and 55 °C are practically identical and equal to 45.2 Å, whereas for a pure 16:0 PSM bilayer they find peak-to-peak distance to be 46.9 Å at 29 °C and 44.4 Å at 50 °C.[7] In their earlier study of a pure 18:0 SM bilayer system at various temperatures and levels of hydration Maulik *et al.*[6] established that for the highest hydration levels (greater than 25 wt % H_2O) 18:0 SM has a chain melting phase transition at 45 °C. For pure 18:0 SM Maulik *et al.* also estimate the area per molecule to be 45 $Å^2$/mol at 22 °C and 55 $Å^2$/mol at 55 °C. Mannock *et al.*[22] investigated the effects of natural and enantiomeric CHOL on egg SM and established that

a)Electronic mail: scotth@iit.edu

incorporation of increasing quantities of CHOL into SM bilayers results in small shifts in the temperature and a large decrease in the enthalpy and cooperativity of the gel-liquid-crystalline phase transition, with this phase transition being completely abolished at 50 mol % CHOL. In x-ray diffraction studies of mixtures of bovine brain SM, DOPC, and CHOL, Gandhavadi *et al.*[30] find electron density peak separations of 48 Å for 2:1 bovine brain SM:CHOL and 43 Å for 1:1:1 DOPC:bovine brain SM:CHOL.

As lipid bilayer simulations became increasingly larger and more complex in scope and scale, several groups have used simulations to examine lipid–cholesterol interactions at an atomic level.[31] Hofsäß *et al.*[32] carried out molecular dynamics simulations of large dipalmitoyl phospatidyl choline (DPPC)–CHOL bilayers at several CHOL concentrations. They found that CHOL reduces the area per phospholipid and increases the ordering of the hydrocarbon chains. Further, they found that the change in order parameters is not uniform, i.e., that the effect of CHOL addition varies with the depth in the bilayer.

Recently Chiu *et al.* reported the results of a comprehensive atomic level simulation study of DPPC–CHOL bilayers at nine different CHOL concentrations.[33] The major finding in this work was a linear relation between the total system area and the CHOL concentration between 50% and ~12% CHOL. This set of simulations provided a picture of the liquid ordered phase in DPPC–CHOL in which a single CHOL can on average partially or fully order, by direct and indirect contact, as many as eight or nine DPPC molecules.

While no simulations have yet appeared for a SM–CHOL bilayer, Mombelli *et al.*[34] have used molecular dynamics to study hydrogen-bonding of pure PSM in solution and in a bilayer assembly. They found that, in solution, PSM amide (NH) and hydroxyl (OH) moieties were extensively involved in forming intramolecular hydrogen bonds with ester oxygens of the phosphate headgroups. In their PSM bilayer simulation Mombelli *et al.* found that 48% of the sphingosine NH groups and 40% of the OH groups became involved in intermolecular hydrogen-bonding. They also found that amide hydrogens and phosphate methyl oxygens participate in relatively few intramolecular hydrogen bondings. Chiu *et al.* have carried out a simulation of a large pure 18:0 SM bilayer consisting of 1600 SM and 50 592 waters.[35] They found that about 57% of the SM molecules participate in intramolecular hydrogen bonding between one of the phosphate ester oxygens and the hydroxyl hydrogen. This work, in addition to characterizing structural properties of SM bilayers (order parameters, electron density, radial distribution functions, and undulation fluctuation spectra), produced a robust force field and simulation methodology for SM bilayer.

The purpose of this paper is to extend the earlier simulations of pure SM[35] to describe combined Monte Carlo and molecular dynamics (MD) simulations of hydrated 18:0 SM–CHOL bilayer systems at 20 and 50 °C. We compare high and low temperature bilayers with each other and with the experimental data available. We also compare our results with experimental and simulated properties of pure SM and DPPC–CHOL bilayer systems.

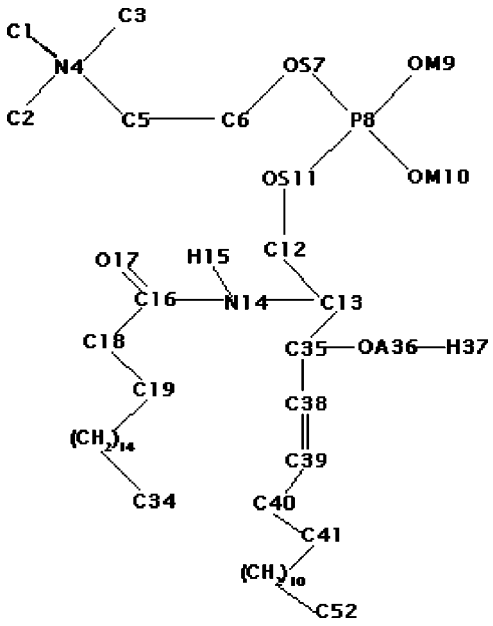

FIG. 1. 18:0 SM molecule, showing the atom numbering scheme used.

SIMULATION METHODS AND PROCEDURES

For all MD and energy minimization procedures we used the GROMACS code package.[36] Analysis of the properties of the systems were done using a combination of GROMACS utilities and our own analysis code. CBMC simulation was done using our own simulation code. Figure 1 shows a diagram of the 18:0 SM molecule, with the atom numbering scheme we used. We constructed our SM–CHOL bilayer from a previously equilibrated hydrated bilayer of 400 SM plus 12 800 water molecules by replacing selected SM molecules with CHOL molecules. The resulting bilayer consisted of 266 SM, 122 CHOL, and 11861 water molecules. The system was equilibrated using our previously published procedure of alternating short (30 ps) molecular dynamics (MD) runs with 20 000 configurational bias Monte Carlo (CBMC) steps.[37] Energy minimization was carried out after each CBMC run. All initial MD/CBMC runs were performed at 50 °C, with a constant isotropic pressure of 1 atm (zero applied surface tension). Temperature was maintained by weak coupling via the Berendsen method.[38] The bilayer was equilibrated for 3 ns of MD with velocity reset after every MD–CBMC cycle. Then a continuous 7 ns MD trajectory was run for the system.

After reaching a total of 10 ns at 50 °C, we lowered the temperature to 20 °C keeping all other run parameters fixed. Then we re-equilibrated the bilayer using the same alternating MD/CBMC procedure described above for 3 ns, and finally, we performed continuous 7 ns MD trajectory for the system. The time step used for the MD runs was 3 fs with all bond length and angles constrained.

Initially cutoffs of 18 and 20 Å were employed for van der Waals and electrostatic interactions, respectively. Neutral charged groups were used. A recent study, published while we were analyzing our simulation data, suggested that truncation of electrostatic interactions in a simulation of a lipid bilayer leads to significant artifacts.[39] In this study of bilay-

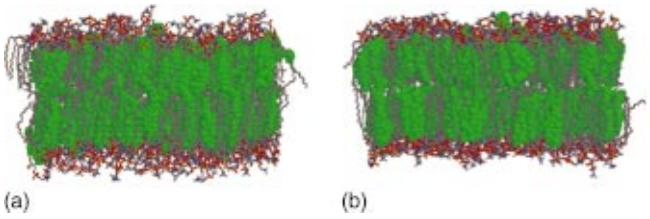

FIG. 2. (Color) (a) Snapshot of 20 °C 18:0 SM–CHOL bilayer. (b) Snapshot of 50 °C 18:0 SM–CHOL bilayer. CHOL molecules are colored in green and are shown space filled. SM molecules are shown as sticks. P atoms on lipid head group are shown in yellow, O atoms in red, N atoms in blue, H atoms in white, C atoms in gray. Water molecules are excluded for clarity.

ers of 128 DPPC molecules plus about 30 water per DPPC simulations were carried out using cutoffs for electrostatics of 1.8, 2.0, and 2.5 nm. Charge groups were not electrically neutral. Data from the simulations were compared with a simulation of the same system using particle- mesh Ewald (PME) summation for the long range electrostatic interactions. Several major differences emerged between the cutoff-based simulations and the PME-based simulation. For example, the area per molecule converged to 0.55 nm^2 for the 1.8 nm cutoff run, to 0.60 nm^2 for the 2.0 nm cutoff run, and to 0.65 nm^2 for the 2.5 nm cutoff run, the latter value being consistent with the area reached by the PME run. Also, spurious peaks were found in radial distribution functions between N–N and P–P pairs of DPPC polar group molecules at the cut-off distance. These peaks were not evident in PME calculations.

The existence of artifacts due to the treatment of electrostatic interactions is a function of many variables, including the cutoff range, the use of non-neutral charge groups, and the number of charged atoms per molecule. After testing for the existence of artifacts, we found that the area per molecule in our SM–CHOL simulations was sensitive to the use of cutoffs, and increased when we performed molecular dynamics runs using particle-mesh Ewald summation for the long-range effects of electrostatic interactions. Accordingly we restarted our simulations of both high and low temperature systems using the PME method for long-range electrostatic corrections using a cutoff of 0.9 nm in the direct space and a Fourier spacing of 0.11 nm. Both simulated systems were run for another 10 ns under the *NPT* boundary conditions with Parrinello–Rahman pressure coupling.[40,41] The neighbor pain list was updated every 4 time steps (12 fs). All the force field parameters used in this study are identical to the force field parameters used by our group for studying pure 18:0 SM bilayer (also simulated using PME for the long-range electrostatic corrections).[35] Properties of the systems described in this paper were calculated over the final 3 ns of the PME-based runs.

RESULTS

Figure 2 shows final snapshots of both high and low temperature bilayers after 10 ns. Visual comparison of the snapshots shows that the overall qualitative structure of both systems is very similar. Equilibration for these bilayers is demonstrated in Fig. 3, which shows plots of the area per molecule versus time for both systems over the last 3 ns. The stability of both simulations is revealed in the near-flatness, within fluctuations, of the plots. For the high temperature bilayer the time-averaged area per molecule is 43.9 $Å^2$/mol. For the low temperature bilayer the time-averaged area per molecule is 43.7 $Å^2$/mol. Comparison with simulations of a 2:1 DPPC–CHOL bilayer published earlier by our group reveals that area per molecule is slightly higher for the SM–CHOL bilayer than for the DPPC–CHOL bilayer at a similar CHOL concentration. Figure 3 shows that, within fluctuations, these areas are the same for the two systems. Interestingly, the area per molecule for a simulated DPPC–CHOL system at 50 °C temperature and 2:1 lipid–cholesterol ratio was smaller, 40 ± 1 $Å^2$/mol.[33,42] This suggests that the DPPC chains are better able to solvate the hydrophobic CHOL molecules. The double bond at the 3–4 position on the sphingosine chain likely contributes to the larger area for SM–CHOL compared to DPPC–CHOL at the same temperature and concentration. The double bond, while oriented roughly perpendicular to the bilayer plane, adds additional rigidity to the SM molecules, compared to DPPC. Comparison of the high temperature bilayer area per molecule profile with that of a pure 18:0 SM bilayer simulated at 50 °C[35] reveals that 31% CHOL concentration leads to a decrease in the area per molecule of 8 $Å^2$/mol.

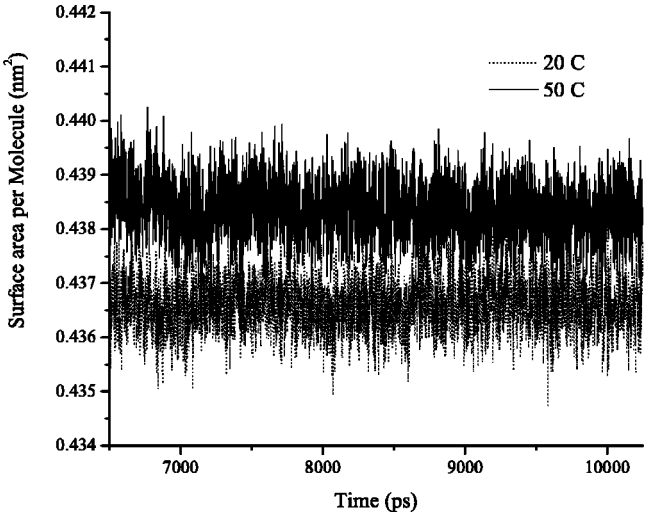

FIG. 3. Plot of the area per molecule for both 20 and 50 °C SM–CHOL bilayers vs time over the last 5 ns of simulation.

Using the procedure described by Hofsäß *et al.*[32] we have calculated the area per SM and CHOL molecules separately. The area per SM is given by[32]

$$A_{\mathrm{SM}} = \frac{2A_{\mathrm{BOX}}}{(1-x)N_{\mathrm{LIP}}}\left(1 - \frac{xN_{\mathrm{LIP}}V_{\mathrm{CHOL}}}{V_{\mathrm{BOX}} - N_{\mathrm{WAT}}V_{\mathrm{WAT}}}\right),$$

where A_{SM} is the area per SM molecule, A_{BOX} and V_{BOX} represent the *xy* area and the volume of the simulation box, respectively, N_{WAT} is the number of water molecules in the system, N_{LIP} is the total number of lipid molecules (i.e., $N_{\mathrm{SM}} + N_{\mathrm{CHOL}} = 388$). $x = N_{\mathrm{CHOL}}/N_{\mathrm{LIP}}$ represents the fraction of CHOL molecules in the system. V_{WAT} and V_{CHOL}, the

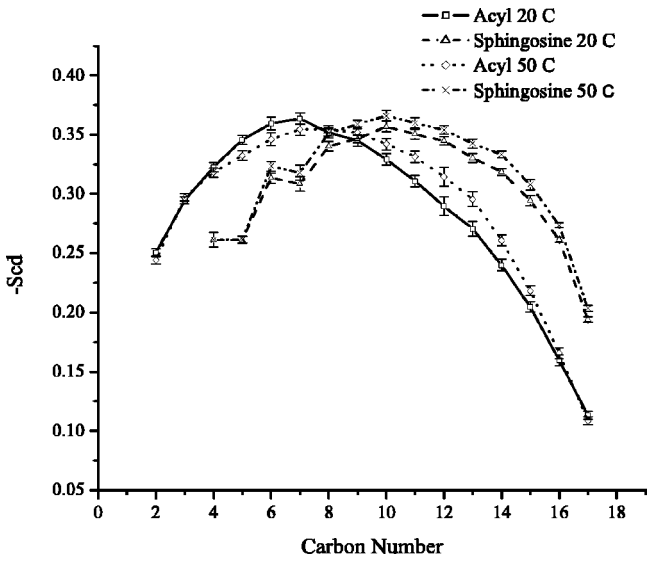

FIG. 4. Plot of the SM chain order parameter profiles for 20 and 50 °C SM–CHOL bilayers.

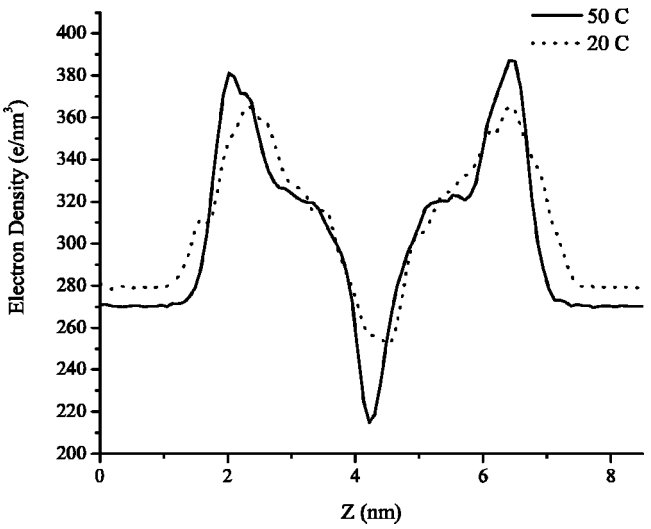

FIG. 5. Plot of the electron density profiles for 20 and 50 °C SM–CHOL bilayers.

volume of single water and CHOL molecules, were taken to be 0.030 and 0.593 nm^3, respectively.[32] The area per CHOL, A_{CHOL}, can be obtained using the formula.[32]

$$A_{\mathrm{CHOL}}=\frac{2A_{\mathrm{BOX}}V_{\mathrm{CHOL}}}{V_{\mathrm{BOX}}-N_{\mathrm{WAT}}V_{\mathrm{WAT}}}.$$

For the 20 °C simulation we find $A_{\mathrm{SM}}=0.513\ \mathrm{nm}^2$, $A_{\mathrm{CHOL}}=0.272\ \mathrm{nm}^2$; for 50 °C we find $A_{\mathrm{SM}}=0.516\ \mathrm{nm}^2$, $A_{\mathrm{CHOL}}=0.268\ \mathrm{nm}^2$. In crystalline cholesterol the molecular area is $\sim$0.37–0.38 nm^2.[43,44] The area per cholesterol is expected to be lower in bilayer mixtures compared to crystalline systems, where rigid cholesterol molecules cannot fill space as efficiently as the flexible lipid chains allow them in bilayer. Chiu *et al.*[33] found the area per CHOL in DPPC–CHOL mixtures at 50° to be 0.223 nm^2 for the range of CHOL concentrations from 12.5% to 50%. Hofsäß *et al.* also found the area per CHOL in DPPC–CHOL bilayer systems simulated at 50 °C to be approximately independent of CHOL concentration and equal to $0.27\pm0.1\ \mathrm{nm}^2$. Our results for SM–CHOL indicate that the area per CHOL in SM–CHOL is absolutely the same as in DPPC–CHOL mixtures.

Figure 4 shows order parameter profiles for SM acyl and sphingosine chains calculated for both high and low temperature bilayers. Within error bars the profiles for 20 and 50 °C systems are identical, which indicates near-identical ordering of SM hydrocarbon chains in both systems. It is useful to compare these profiles with SM acyl and sphingosine chain order parameters for the pure SM system simulated at 50 °C:[35] for pure SM, carbons near the top of the acyl chain have $-S_{\mathrm{CD}}\sim0.3$, whereas for SM–CHOL bilayers the profile for the same carbons shows more ordering (the order parameters for sixth and seventh carbon are $\sim$0.35). There is also a significant difference in the sphingosine chain order parameter profiles—for the carbons in the middle of the sphingosine chain we observe greater order parameters in SM–CHOL than in the pure SM system.[35] However for both acyl and sphingosine chains, the order parameters at initial and terminal carbons show no difference between SM–CHOL and pure SM bilayers.

In Fig. 5 we plot the calculated electron density profiles for both systems. We find a peak to peak separation of 42 Å with an estimated error of ±2 Å for both the high temperature system and the low temperature system. This value is less than the 48 Å peak separation measured by Gandhavadi *et al.*[30] for 2:1 bovine brain SM:CHOL. The difference is in part due to the heterogeneous composition of bovine brain SM, in particular to the presence of long saturated chains (27% 24:0 SM). In our pure SM simulation[35] we found a peak-to-peak separation of 41 Å, so that the inclusion of 31% cholesterol has produced a very small apparent thickening of the bilayers. Since this difference is smaller than might be anticipated, we have examined the extent of chain interdigitation of SM near-terminal methylenes as well as interdigitation of CHOL terminal methyls and CHOL hydrocarbon tail methylenes between the two leaflets. To this end we have calculated atom distributions for each leaflet separately. We found that the distributions of SM near-terminal methylenes for the two leaflets overlap to an extent that about 10% of all methylenes are in the overlap region in the center of the bilayer. For the pure 18:0 SM bilayer simulated at 50°[35] it was found that only $\sim$2% of all methylenes overlap in the bilayer center. We also found that 7% of all CHOL terminal methyls and only 0.6% of all CHOL methylenes overlap in the bilayer center. These results indicate that interdigitation is slightly more prominent in SM–CHOL systems than in pure SM bilayers. This result may partially explain the fact that simulated 18:0 SM–CHOL bilayers are thinner than experimental PSM–CHOL bilayers,[7] and are only about 1 Å thicker than our simulated pure SM bilayer.

Maulik *et al.*[7] obtain a value of peak-to-peak electron density thickness of 45.2 Å for 1:1 16:0 PSM–CHOL over a 26 °C temperature range, at both 29 and 55 °C. Our simulated systems are thus also thinner than experimental 1:1 PSM–CHOL bilayers.[7] It is possible that interdigitation does not occur in the shorter-chain PSM–CHOL bilayers at 50%

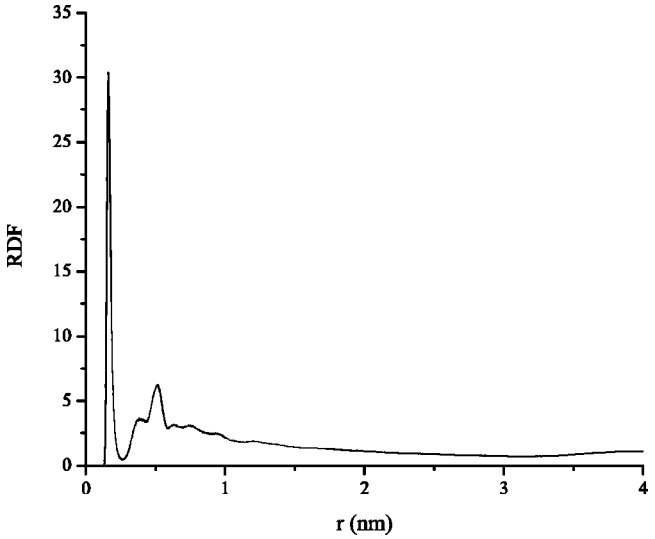

FIG. 6. Plot of rdf between CHOL hydroxyl hydrogens and SM carbonyl oxygens (O17).

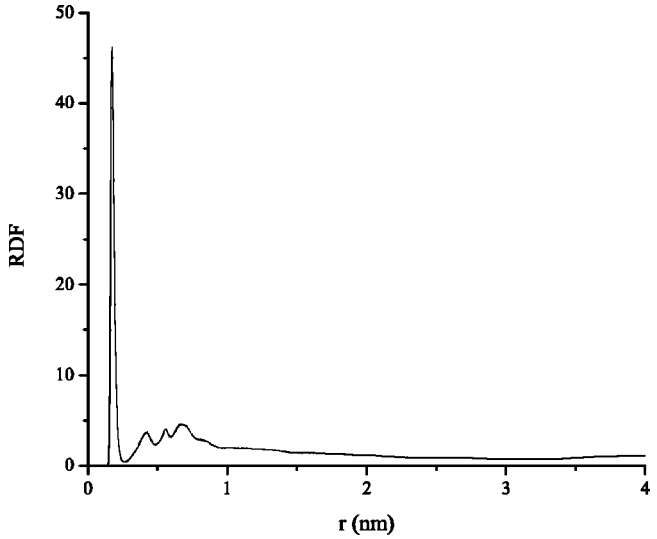

FIG. 7. Plot of rdf between CHOL hydroxyl oxygens and SM amide hydrogens (H15).

CHOL concentration. Maulik *et al.*[6] obtain a peak-to-peak distance of 41 Å for pure 18:0 SM at 50 °C at all hydration levels between 20 and 50 wt %. Comparison of the simulation data with these results suggests that addition of 31% CHOL has little effect on the thickness of the SM bilayer. For 16:0 PSM, Maulik *et al.*[7] found that at 55 °C addition of 50% CHOL to the bilayer caused an increase in the peak-to-peak distance of only 0.8 Å.

In order to analyze hydrogen bonding between SM and CHOL molecules, we have calculated radial distribution functions (rdfs) between pairs of atoms likely to participate in this process. Using a somewhat coarse-grained definition, we associate all hydrogen–oxygen atom pairs whose interatomic distance lies within rdf peaks of ~2 Å or less with hydrogen bonds. The rdf between atom *x* and atom *y* is defined as the average over all *x* atoms in the system of the distance from an *x* atom to all *y* atoms up to the interaction range cutoff. The distances between designated atoms on different molecules were binned, and the resulting rdf was normalized by dividing by $4\pi r^2 dr$ where *r* is the mid-bin distance variable and *dr* is the bin width, set at 0.5 Å. We have carried out rdf calculations for both high and low temperature systems, and we find that rdf profiles for our two systems are nearly identical. Hence, we show only the results for the 50 °C bilayer. Figure 6 shows the rdf between CHOL hydroxyl hydrogens (H1) and SM carbonyl oxygens (O17). The sharp peak at about 2 Å is due to hydrogen bonding between H1 and O17 atoms. The overall shape of the curve is a measure of the range of the ordering induced by the carbonyl O–CHOL OH interaction, with secondary peaks indicative of long-range structure in the bilayer. The curve shows a small secondary peak and almost no structure beyond 5 Å. Calculation of number of atoms in the first coordination shell around the CHOL H1 reveals that 18.4% of all CHOL H1 are on average hydrogen bonded to SM carbonyl oxygen atoms. The CHOL hydroxyl group is also capable of hydrogen bonding with the SM amide group through the CHOL O and SM H15 atoms. Figure 7 illustrates the rdf for these atoms. Once again, the strong peak at 2 Å indicates hydrogen bonding between these atoms. We find that 14.3% of all CHOL O are on average hydrogen bonded to SM amide hydrogen atoms. It must be mentioned that, due to the close location of O17 and H15 atoms in SM molecules, the calculated values for H1–O17 and O–H15 pairs are not independent and should not be taken separately. Figures 8 and 9 show two more rdfs involving the CHOL hydroxyl hydrogen: H1 and SM hydroxyl oxygen atoms (OA36) and between H1 and SM methyl oxygens (OM9–OM10). The plots reveal hydrogen bonding between these atom pairs as well (10.8% for H1–OA36, 6.9% for H1–OM9, and 3.8% for H1–OM10). Figure 10 illustrates rdf profiles between CHOL H1 and SM ester oxygens (OS7 and OS11, together). Hydrogen bonding between these atoms occurs, however the percentage of hydrogen bonding is smaller (1.8% for H1–OS7 and 0.7% for H1–OS11). Instead, stronger secondary peaks

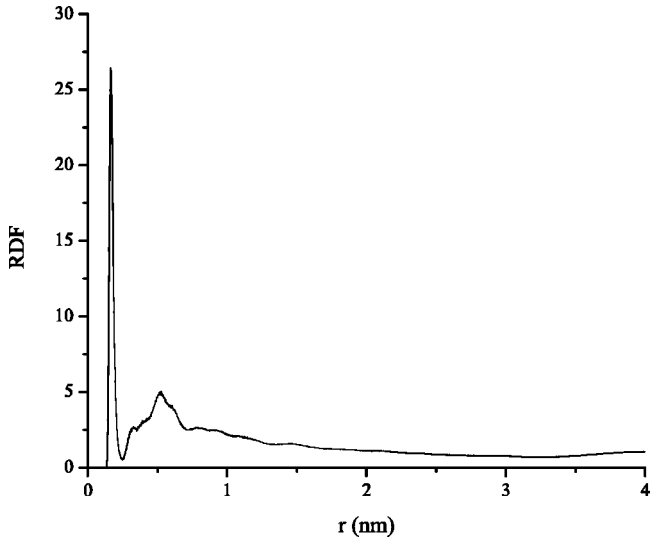

FIG. 8. Plot of rdf between CHOL hydroxyl hydrogens and SM hydroxyl oxygens (OA36).

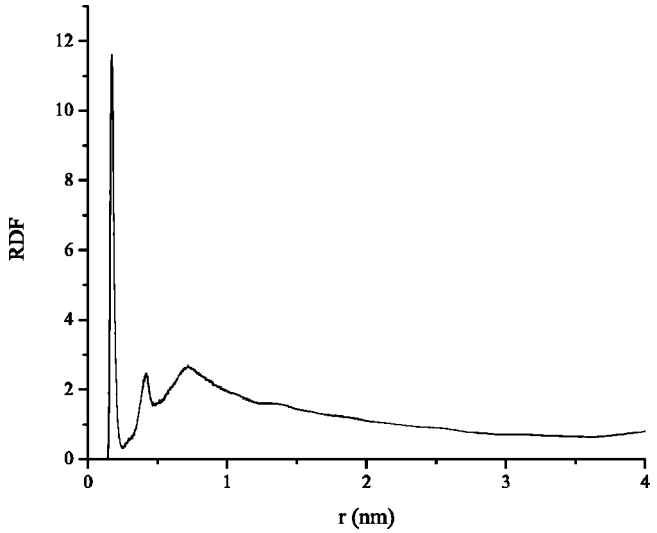

FIG. 9. Plot of rdf between CHOL hydroxyl hydrogens and SM methyl oxygens (OM9–OM10).

merge and the structure extends to almost 10 Å. We have also calculated rdfs between different groups on SM molecule as well as between SM and water molecules and CHOL and water molecules. In Table I we summarize the hydrogen bond percentages we have calculated and compare them with pure SM data obtained from an earlier 18:0 SM bilayer simulation study.[35] As was expected there is a significant decrease in hydrogen bonds between SM O17–H15 atoms on different SM molecules. Almost 50% fewer O17 and H15 participate in intermolecular hydrogen bonding when cholesterol is present in the system. On the other hand, intermolecular hydrogen bonding between OA36 and H15 atoms, and intramolecular hydrogen bonding between H37–OS7 atoms, are not effected by the presence of cholesterol in the system. We find that intramolecular hydrogen bonding between H37 and OS11 atoms has increased compared to the pure SM system. It is of interest to investigate how the hydration of the SM polar group is effected by the addition of

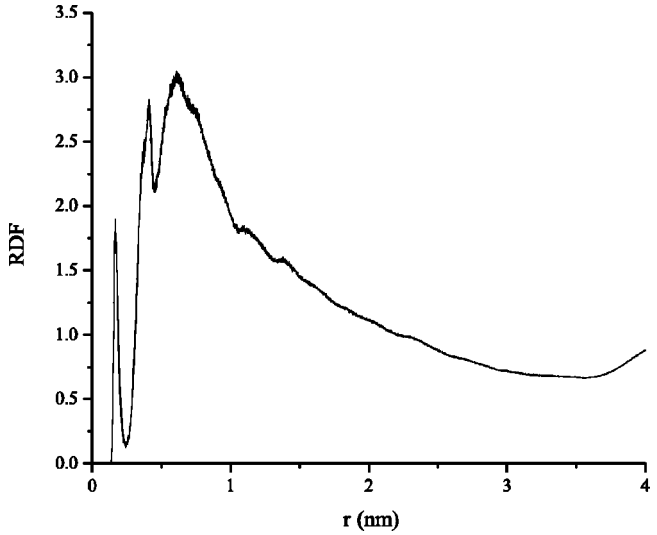

FIG. 10. Plot of rdf between CHOL hydroxyl hydrogens and SM ester oxygens (OS7–OS11).

TABLE I. Number of hydrogen bonds per molecule for various donor/acceptor sites.

	Atom pairs	SM–CHOL	Pure SM
CHOL–SM	H1–O17	0.184	
CHOL–SM	O–H15	0.143	
CHOL–SM	H1–OA36	0.108	
CHOL–SM	H1–OM9	0.069	
CHOL–SM	H1–OM10	0.038	
CHOL–SM	H1–OS7	0.018	
CHOL–SM	H1–OS11	0.007	
SM–water	OM9 or OM10–HW	0.70	1.14
SM–water	OS7–HW	0.36	0.49
SM–water	OS11–HW	0.09	0.24
SM–water	H15–OW	0.44	0.39
SM–water	OA39–HW	0.52	0.93
SM–water	H37–OW	0.04	0.11
CHOL–water	H1–OW	0.68	
CHOL–water	O–HW	0.44	
Intermolecular(SM)	O17–H15	0.15	0.30
Intermolecular(SM)	OA36–H15	0.11	0.11
Intramolecular(SM)	H37—OS11	0.71	0.57
Intramolecular(SM)	H37–OS7	0.01	0.02

cholesterol. From Table I we see that there is substantial decrease in SM polar group hydration when the cholesterol is present in the system. Calculation of hydrogen bonds between CHOL hydroxyl groups and water molecules reveals that 68% of CHOL H1 atoms participate in hydrogen bonding with water and 44% of CHOL O atoms form hydrogen bonds with water molecules.

In order to address the issue of the lateral organization of CHOL in SM–CHOL bilayers and compare with DPPC–CHOL bilayers we studied the time evolution of the rdf between CHOL oxygens. Although we find peaks at distances of 5, 9, and 13 Å, the pattern remains unchanged throughout the simulation. For DPPC–CHOL mixtures,[33] at relatively low concentrations (4%–25%) the similar study showed a gradual emergence of peaks at 5, 10, and 15 Å during the 5 ns run, however at 50% cholesterol concentration no time evolution was observed.

DISCUSSION

The simulations reported in this paper, to our knowledge, are the first for a sphingomyelin–cholesterol bilayer. Our goal was to obtain atomic-resolution structural data for this system, and compare SM–CHOL domains at 20 and 50 °C. Our simulations show that at both 20 and 50 °C, SM–CHOL bilayers are very similar in structure. The electron density profiles show that both domains are characterized by the same bilayer thickness. Comparison of SM acyl and sphingosine chain order parameters for high and low temperature bilayers reveals that the degree of ordering of lipid chains is the same in both 20 and 50 °C domains despite the 30° temperature interval. This result is interesting in light of the fact that at 20 °C a pure SM bilayer would be in the gel phase whereas at 50 °C a pure SM bilayer is in the fluid phase. Comparison of order parameter profiles of the 50 °C SM–CHOL system with that of pure SM bilayer simulated at the same temperature indicates that the lipid chains are more ordered when CHOL is present in the system. We conclude

that the two simulated SM–CHOL domains are both found in an intermediate state of fluidity, consistent with a liquid ordered phase. The fact that CHOL incorporation into the model lipid membranes causes broadening and eventual elimination of the cooperative gel-to-liquid-crystalline phase transition is well documented in the literature. Our simulations are consistent with this observation. This intermediate state of fluidity may be necessary for the binding of proteins and other molecules which associate with raft domains.

Calculated radial distribution functions reveal important features of SM–CHOL interactions. CHOL hydroxyl groups exhibit hydrogen bonding with the SM carbonyl and methyl oxygens, and with amide hydrogens and hydroxyl oxygens. There is relatively little tendency for CHOL to form hydrogen bonds with SM ester oxygens. These results are consistent with simulations of pure PSM.[34] Mombelli and coworkers[34] also found that PSM hydroxyl moieties and ester oxygens are extensively involved in intra- and intermolecular hydrogen bonding, whereas carbonyl and phosphate oxygens are not strongly involved in this process. Compared to DPPC–CHOL bilayers, in a SM–CHOL bilayer there are additional hydrogen bonding possibilities for the cholesterol hydroxyl group. This may explain the high affinity of the CHOL hydroxyl group toward the polar regions of SM molecules. Our simulations also show that the CHOL hydroxyl group is extensively involved in hydrogen bonding with water molecules. This result, along with intramolecular hydrogen bonding has the effect of reducing the hydration of the polar region in SM lipid. The result that polar regions of SM lipids in bilayer systems are less hydrated than polar regions of DPPC lipids is consistent with a recent experimental study of the hydration state of the interfacial region of DPPC, 16:0 SM, and 16:0 dihydrosphingomyelin (DHSM) vesicles using fluorescence spectroscopy.[28] In this study, using dansyl-PE probe Nyholm *et al.*[28] showed that the degree to which polar groups were exposed to water in the membranes increased in the order: 16:0 SM$<$DPPC$<$16:0 DHSM.

ACKNOWLEDGMENTS

We thank Sagar A. Pandit for comments on the manuscript and for many insightful discussions. Research is supported by National Institutes of Health Grant No. GM54651. The parallel version of the CBMC code was written by Aron Ahmadia.

[1] P. L. Yeagle, *The Membranes of Cells* (Academic, San Diego, 1993).
[2] M. R. Vist and J. H. Davis, Biochemistry **29**, 451 (1990).
[3] T. P. W. McMullen and R. N. McElhaney, Curr. Opin. Colloid Interface Sci. **1**, 83 (1996).
[4] T. J. McIntosh and S. A. Simon, Biochemistry **28**, 17 (1989).
[5] L. Finegold, *Cholesterol in Membrane Models* (CRC Press, Boca Raton, FL, 1993).
[6] P. R. Maulik, P. K. Sripada, and G. G. Shipley, Biochim. Biophys. Acta **1062**, 211 (1991).
[7] P. R. Maulik and G. G. Shipley, Biochemistry **35**, 8025 (1996).
[8] D. Needham and R. S. Nunn, Biophys. J. **58**, 997 (1990).
[9] T. Harder and K. Simons, Curr. Opin. Cell Biol. **9**, 534 (1997).
[10] K. Simons and E. Ikonen, Nature (London) **387**, 569 (1997).
[11] R. E. Brown and E. London, J. Membr. Biol. **164**, 103 (1998).
[12] S. Manes, E. Mira, C. Gomez-Moulton, R. A. Lacalle, P. Keller, J. P. Labrador, and A. C. Martinez, EMBO J. **18**, 6211 (1999).
[13] M. J. Aman and K. S. Ravichandran, Curr. Biol. **10**, 393 (2000).
[14] R. Xavier, T. Brennan, Q. Li, C. McCormack, and B. Seed, Immunity **6**, 723 (1998).
[15] M. Kawabuchi, Y. Satomi, T. Takao, Y. Shimonishi, S. Nada, K. Nagai, A. Tarakhovsky, and M. Okada, Nature (London) **404**, 999 (2000).
[16] A. L. Rozelle, L. M. Machesky, M. Yamamoto, H. Driessens, R. H. Insall, M. G. Roth, K. Luby-Phelps, G. Marriot, A. Hall, and H. L. Yin, Curr. Biol. **6**, 311 (2000).
[17] K. H. Cheong, D. Zachetti, E. Schneeberger, and K. Simons, Proc. Natl. Acad. Sci. U.S.A. **96**, 6241 (1999).
[18] A. Viola, S. Schroeder, Y. Sakakibara, and A. Lanzavecchia, Science **283**, 680 (1999).
[19] S. N. Manie, S. Debreyne, S. Vincent, and D. Gerlier, J. Virol. **74**, 305 (2000).
[20] T. Harder, P. Scheiffele, P. Verkade, and K. Simoms, J. Cell Biol. **141**, 929 (1998).
[21] B. S̃onnichsen, de Renzis, E. Nielsen, J. Reitdorf, and M. Zerial, J. Cell Biol. **149**, 901 (2000).
[22] D. A. Mannock, T. J. McIntosh, X. Jiang, D. F. Covey, and R. N. McElhaney, Biophys. J. **84**, 1038 (2003).
[23] T. K. M. Nyholm, M. Nylund, and P. Slotte, Biophys. J. **84**, 3138 (2003).
[24] W. Guo, V. Kurze, T. Huber, N. Afdhal, K. Beyer, and J. A. Hamilton, Biophys. J. **83**, 1465 (2002).
[25] A. V. Samsonov, I. Mihalyov, and F. S. Cohen, Biophys. J. **81**, 1486 (2001).
[26] T.-Y. Wang and J. R. Silvius, Biophys. J. **79**, 1478 (2000).
[27] T.-Y. Wang and J. R. Silvius, Biophys. J. **84**, 367 (2003).
[28] T. Nyholm, M. Nylund, A. Soderholm, and J. P. Slotte, Biophys. J. **84**, 987 (2003).
[29] T. P. W. McMullen, R. N. A. H. Lewis, and R. N. McElhaney, Biochemistry **32**, 516 (1993).
[30] M. Gandhavadi, D. Allende, A. Vidal, S. A. Simon, and T. J. McIntosh, Biophys. J. **82**, 1469 (2002).
[31] H. L. Scott, Curr. Opin. Struct. Biol. **12**, 495 (2002).
[32] C. Hofsäß, E. Lindahl, and O. Edholm, Biophys. J. **84**, 2192 (2003).
[33] S.-W. Chiu, E. Jakobsson, R. J. Mashl, and H. L. Scott, Biophys. J. **83**, 1842 (2002).
[34] E. Mombelli, R. Morris, W. Taylor, and F. Fraternali, Biophys. J. **84**, 1507 (2003).
[35] S.-W. Chiu, S. Vasudevan, E. Jakobsson, R. J. Mashl, and H. L. Scott, Biophys. J. **85**, 3624 (2003).
[36] E. Lindahl, B. Hess, and D. van der Spoel, J. Mol. Model. [Electronic Publication] **7**, 306 (2001) (www.gromacs.org).
[37] S.-W. Chiu, M. Clark, E. Jakobsson, S. Subramaniam, and H. L. Scott, J. Comput. Chem. **20**, 1153 (1999).
[38] H. J. C. Berendsen, J. P. M. Postma, A. DiNola, and J. R. Haak, J. Chem. Phys. **81**, 3684 (1984).
[39] M. Patra, M. Karttunen, M. T. Hyvo̊nen, E. Falck, P. Lindqvist, and I. Vattulainen, Biophys. J. **84**, 3636 (2003).
[40] M. Parrinello and A. Rahman, J. Appl. Phys. **52**, 7182 (1981).
[41] S. Nosé and M. L. Klein, Mol. Phys. **50**, 1055 (1983).
[42] S.-W. Chiu, E. Jakobsson, and H. L. Scott, J. Chem. Phys. **114**, 5435 (2001).
[43] H.-S. Shieh, L. G. Hoard, and C. E. Nordman, Acta Crystallogr., Sect. B: Struct. Crystallogr. Cryst. Chem. **37**, 1538 (1981).
[44] B. M. Craven, Acta Crystallogr., Sect. B: Struct. Crystallogr. Cryst. Chem. **35**, 1123 (1979).